DOI: 10.1002/ejic.200800055

Crystal Structure and Magnetism of the 6H Hexagonal Double Perovskites Ba_2FeSbO_6 and $Ba_2CoSbO_{6-\delta}$: A Neutron Diffraction and Mössbauer Spectroscopy Study

M. Retuerto,[a] J. A. Alonso,*[a] M. J. Martínez-Lope,[a] M. García-Hernández,[a] K. Krezhov,[b] I. Spirov,[b] T. Ruskov,[b] and M. T. Fernández-Díaz[c]

Keywords: Antisite disorder / Spin glass / Hexagonal perovskites / Crystal structures / Defective perovskites / Oxygen deficiency

$Ba_2MSbO_{6-\delta}$ (M = Fe, Co) double perovskites have been prepared in polycrystalline form by the solid-state reaction in air and characterized by X-ray diffraction (XRD), neutron powder diffraction (NPD), magnetic measurements and Mössbauer spectroscopy (for M = Fe). At room temperature, the crystal structure of both compounds can be defined as a 6-layered (6H) hexagonal perovskite structure (space group $P6_3/mmc$), with a = 5.7875(1) Å and c = 14.2104(2) Å for M = Fe and a = 5.7548(2) Å and c = 14.1439(7) Å for M = Co. M and Sb cations are randomly distributed over *4f* and *2a* Wickoff positions. The crystal structure is constituted by dimer units of $(M,Sb)_{4f}O_6$ octahedra sharing a face along the c axis; the dimers, which sharing corners, are connected by a single layer of $(M,Sb)_{2a}O_6$ octahedra. A severe degree of antisite disordering was detected in the Fe compound, which indicates the presence of 52.8% Fe:47.2% Sb at the $(Fe,Sb)_{2a}$ positions, whereas for Co, 64.0% Sb is present at the $(Co,Sb)_{2a}$ sites. Mössbauer spectroscopic data for Ba_2FeSbO_6 confirm the existence of two distinct crystallographic sites for Fe^{3+}. One site corresponds to very regular FeO_6 octahedra (at *2a* positions), which gives rise to a singlet in the Mössbauer spectra at room temperature and 77 K that is broadened by the strong Fe/Sb disorder over this site. The second environment for Fe^{3+} contributes to a broadened doublet in the Mössbauer spectra, which corresponds to a very distorted FeO_6 octahedron (at *4f* sites), for which neutron powder diffraction data demonstrates an axial distortion with two sets of Fe–O distances. This distortion is due to the repulsion of the highly charged Sb^{5+} cations within the dimer units of the $(Fe,Sb)_{4f}O_6$ octahedra, and it is much reduced in the Co compound, where the amount of Sb^{5+} at these sites is smaller. Magnetic measurements suggest the absence of long-range magnetic ordering for both samples, which is confirmed by low-temperature neutron diffraction data.

Introduction

Since the discovery of colossal magnetoresistance in Sr_2FeMoO_6[1] and Sr_2FeReO_6,[2,3] double perovskites with the general stoichiometry $A_2B'B''O_6$ (A = alkali earth metals; B′, B″ = transition metals) have been the topic of a large number of studies over the last few years. This effect is of technological interest for the detection of magnetic fields and in magnetic memory devices.[4,5] These materials are half-metallic ferromagnets with T_Cs that are significantly above room temperature.

In addition to the second- and third-row transition metals such as Mo, Re and W, some p block elements such as Sb or Te can also be successfully stabilized at the B″ crystallographic positions of some double perovskites, since Sb^{5+} and Te^{6+} cations exhibit the required spherical symmetry and ionic size. We have recently synthesized some members of the $A_2B'SbO_6$ family: Ca_2CrSbO_6 and Sr_2CrSbO_6 double perovskites were prepared and investigated by magnetic measurements and neutron powder diffraction (NPD) data. Sr_2CrSbO_6 is an antiferromagnet with a Néel temperature of 12 K, whereas Ca_2CrSbO_6 exhibits ferromagnetic long-range order below T_C = 16 K.[6,7]

As the tolerance factor of the perovskite structure decreases from unity, the cubic symmetry (space group $Fm\bar{3}m$ with a rock-salt-like distribution of the B′ and B″ cations over the B sites of the perovskite) is typically reduced to tetragonal (space group $I4/m$) or even monoclinic ($P2_1/n$) as a result of the tilting of the $B'O_6$ and $B''O_6$ octahedra. On the other hand, when the perovskite tolerance factor is greater than unity, the crystal structure tends to evolve from cubic to hexagonal. The prototypical hexagonal distortion of the perovskite originally found in one of the polymorphs of $BaTiO_3$[8] is the so-called 6H structure, defined in the $P6_3/mmc$ space group. For double perovskites, this structural arrangement contains two non-equivalent B′ and B″

[a] Instituto de Ciencia de Materiales de Madrid, C.S.I.C., Cantoblanco, 28049 Madrid, España
[b] Institute of Nuclear Research and Nuclear Energy, Bulgarian Academy of Sciences, 72 Tsarigradsko Chaussee Boulevard, 1784 Sofia, Bulgaria
[c] Institut Laue Langevin, B. P. 156X, 38042 Grenoble, France

cations at octahedral positions in a 2:1 ratio, and it consists of dimer units of face-shared $B'O_6$ octahedra connected, through common corners, by a single layer of $B''O_6$ octahedra. This hexagonal structure is ideally suited for perovskite oxides with the composition $A_3B'_2B''O_9$ that naturally contain double the amount of B′ cations relative to B″ cations, but can also be adopted by double perovskites with a B′/B″ ratio of 1:1. In these cases, there is an intrinsic disorder at least over the nominal B′ positions, which must contain 1/3 of the B″ atoms. Recently, an oxide with Ba_2CrMoO_6 stoichiometry was shown to exhibit this hexagonal 6H-perovskite structure.[9] In the course of our current research on double perovskite oxides, we have been interested in the Ba_2MSbO_6 (M = Fe, Co) analogues. These perovskites were previously reported in the 1960s by Blasse,[10,11] who described the crystal structure from X-ray diffraction (XRD) data, and the Fe compound was investigated much later by Battle et al.,[12] who reported the absence of antiferromagnetic ordering from macroscopic magnetic measurements. In this paper we aim to complement this preliminary research with a high-resolution NPD investigation of the crystal structures and their thermal evolution, and we also confirm the absence of long-range magnetic ordering for both perovskites. This study is complemented with Mössbauer spectroscopy and macroscopic magnetic measurements, which are discussed in light of subtle structural peculiarities.

Results

X-ray Diffraction

The XRD patterns of Ba_2MSbO_6, M = Fe, Co, are characteristic of a 6H hexagonal polytype perovskite structure. Figure 1 shows the Rietveld plots of a preliminary study from XRD data and displays an excellent agreement between the observed and calculated patterns and the absence of minor impurity phases.

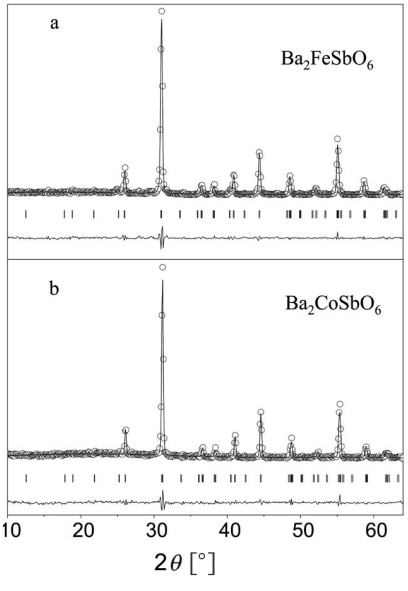

Figure 1. X-ray Powder Diffraction patterns for (a) Ba_2FeSbO_6 and (b) Ba_2CoSbO_6, collected at room temperature with Cu-K_α radiation. The Rietveld fits correspond to the structural model derived from the NPD study.

Neutron Diffraction

The structural refinement of Ba_2MSbO_6 (M = Fe, Co) from room temperature high-resolution NPD data was performed in the space group $P6_3/mmc$ (No. 194), with $Z = 3$, $a = 5.7875(1)$ Å and $c = 14.2104(2)$ Å for M = Fe and $Z = 3$, $a = 5.7548(2)$ Å and $c = 14.1439(7)$ Å for M = Co. There are two independent positions for the Ba atoms; Ba1 is located at *2b*(0,0,1/4) and Ba2 at *4f*(1/3,2/3,*z*) sites. There are also two different crystallographic positions for the B atoms, with different multiplicity: *2a*(0,0,0) and *4f*(1/3,2/3,*z*). The two types of oxygen atoms are at *6h*(*x*,2*x*,1/4) and *12k*(*x*,2*x*,*z*) positions. In a first trial, 2/3 of the M atoms were placed at *2a* sites and 1/3 of the M atoms together with the Sb atoms were randomly

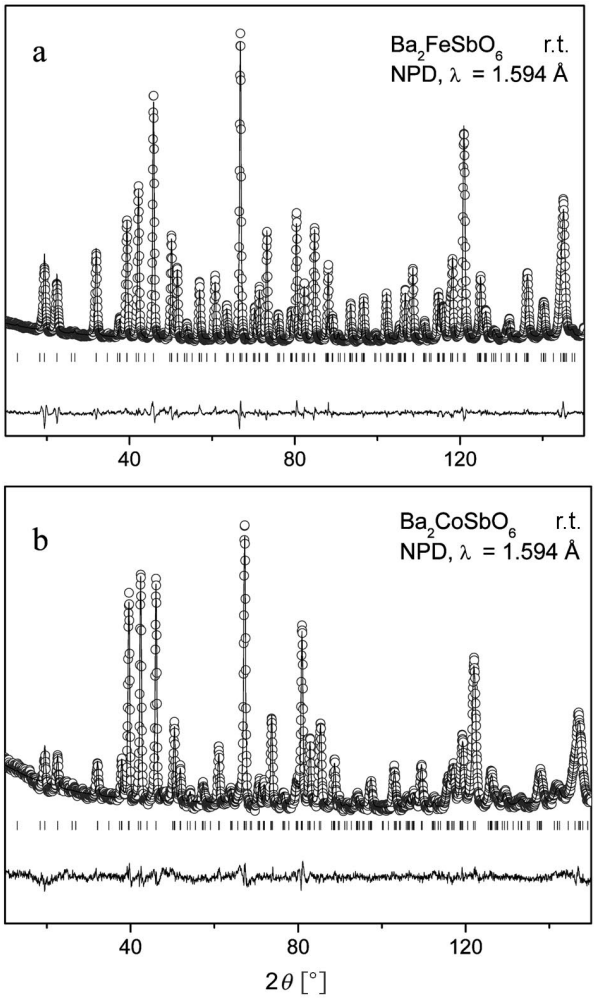

Figure 2. Observed (open circles), calculated (full line) and difference (bottom) NPD Rietveld profiles for (a) Ba_2FeSbO_6 and (b) Ba_2CoSbO_6 at 295 K.

distributed at *4f* positions. Antisite disordering was then refined by assuming that some Sb atoms from the *4f* positions can randomly replace some M atoms at *2a* positions, and vice versa. Linear constraints were applied between the *2a* and *4f* sites, whilst the initial stoichiometry M/Sb = 1:1 was always maintained. The oxygen occupancies were also refined at both O1 and O2 positions. The final crystallographic stoichiometries are $Ba_3(Fe_{0.53(1)}Sb_{0.47(1)})_{2a}(Fe_{0.97(1)}Sb_{1.03(1)})_{4f}O_{8.88(6)}$ and $Ba_3(Co_{0.36(4)}Sb_{0.64(4)})_{2a}(Co_{1.14(4)}Sb_{0.86(4)})_{4f}O_{8.70(6)}$ after the refinement of the room temperature (295 K) data. If we define the degree (in %) of B-cation ordering as $2|0.5 - n|\cdot 100$, where n is the stoichiometric coefficient of Sb in the mentioned formulae, we obtain degrees of ordering of 6% for M = Fe and 28% for M = Co; the cobalt perovskite is substantially more ordered than the iron perovskite. The good agreement between observed and calculated NPD profiles at room temperature is illustrated in Figure 2. Table 1 includes the final atomic coordinates and discrepancy factors after refinement. Table 2 lists the main interatomic distances and angles. The medium-resolution D1A data collected at 97 and 191 K for M = Fe were also refined with the same structural model; the atomic positions and interatomic distances are also included in Table 1 and Table 2, respectively. A drawing of the structure is shown in Figure 3, which highlights the presence of dimer units of $(M,Sb)O_6$ octahedra (M and Sb at *4f* sites) sharing a face through the O1 oxygen atoms. The dimers are connected along the *c* axis by a single $(M,Sb)O_6$ octahedra (at *2a* sites) sharing corners through the O2 oxygen atoms.

Table 1. Positional and thermal parameters for Ba_2MSbO_6 (M = Fe, Co) after a Rietveld refinement of the NPD data collected at T = 100, 200 and 295 K for M = Fe and T = 295 K for M = Co; space group $P6_3/mmc$.

Ba_2MSbO_6	M = Fe	M = Fe	M = Fe	M = Co
T [K]	97	191	295	295
a [Å]	5.7735(1)	5.77800(9)	5.78754(6)	5.7548(1)
c [Å]	14.1781(3)	14.1884(3)	14.2104(2)	14.1439(7)
V [Å^3]	409.29(1)	410.22(1)	412.215(9)	405.66(2)
Ba 2*b*(0,0,1/4)				
B [Å^2]	0.0(1)	0.2(1)	0.66(5)	0.0(1)
Ba *4f*(1/3,2/3,*z*)				
z	0.5964(2)	0.5964(2)	0.5969(1)	0.5968(3)
B [Å^2]	0.5(1)	0.5(1)	0.66(4)	0.8(1)
M,Sb *2a*(0,0,0)				
B [Å^2]	0.4(1)	0.46(9)	0.36(5)	0.0(1)
Occupancy				
M (*2a*)	0.530(2)	0.530(2)	0.530(2)	0.361(6)
Sb (*2a*)	0.470(2)	0.470(2)	0.470(2)	0.639(6)
M,Sb *4f*(1/3,2/3,*z*)				
z	0.1506(1)	0.1509(1)	0.1505(1)	0.1563(4)
B [Å^2]	0.38(8)	0.51(7)	0.77(4)	0.7(1)
O1 *6h*(*x*,2*x*,1/4)				
x	0.4870(6)	0.4863(6)	0.4870(4)	0.4852(9)
B [Å^2]	0.23(8)	0.20(8)	0.64(4)	0.44(9)
Occupancy	0.980(6)	0.980(6)	0.980(6)	0.922(8)
O2 *12k*(*x*,2*x*,*z*)				
x	0.1654(6)	0.1655(6)	0.1660(4)	0.1658(9)
z	0.4193(1)	0.4195(1)	0.41952(8)	0.4195(1)
B [Å^2]	0.31(6)	0.46(6)	0.79(3)	0.53(5)
Occupancy	0.989(6)	0.989(6)	0.989(6)	0.990(6)
Reliability factors				
χ^2	1.51	2.37	3.39	1.97
R_p [%]	4.63	3.96	3.36	3.58
R_{wp} [%]	5.65	5.00	4.35	4.61
R_I [%]	4.60	3.25	2.36	3.28

Table 2. Some selected bond lengths [Å] and angles [°] for Ba_2MSbO_6.

Ba_2MSbO_6	M = Fe	M = Fe	M = Fe	M = Co
T [K]	97 K	191 K	295 K	295 K
Ba1–O1 (×6)	2.890(4)	2.892(4)	2.897(3)	2.881(6)
Ba1–O2 (×6)	2.916(2)	2.920(2)	2.927(2)	2.912(3)
Ba2–O1(×3)	2.824(4)	2.830(3)	2.824(3)	2.822(5)
Ba2–O2(×3)	3.019(4)	3.019(3)	3.028(3)	3.012(5)
Ba2–O2(×6)	2.895(4)	2.898(3)	2.903(3)	2.887(6)
Ba–O	2.906(4)	2.909(3)	2.9133(3)	2.899(5)
$(M,Sb)_{2a}O_6$ octahedra				
$(M,Sb)_{2a}$–O2 (×6)	2.011(3)	2.012(3)	2.019(2)	2.007(4)
$(M,Sb)_{4f}O_6$ octahedra				
$(M,Sb)_{4f}$–O1 (×3)	2.085(3)	2.078(4)	2.091(2)	2.013(5)
$(M,Sb)_{4f}$–O2 (×3)	1.950(4)	1.954(3)	1.950(3)	1.984(6)
$(M,Sb)_{4f}$–$(M,Sb)_{4f}$	2.819(3)	2.812(3)	2.827(3)	2.652(9)
$(M,Sb)_{4f}$–O	2.017(4)	2.016(4)	2.020(3)	1.998(6)
Angles around O				
$(M,Sb)_{4f}$–O1–$(M,Sb)_{4f}$	85.1(1)	85.1(1)	85.1(1)	82.4(4)
$(M,Sb)_{2a}$–O2–$(M,Sb)_{4f}$	175.9(1)	176.2(1)	176.2(1)	178.1(2)

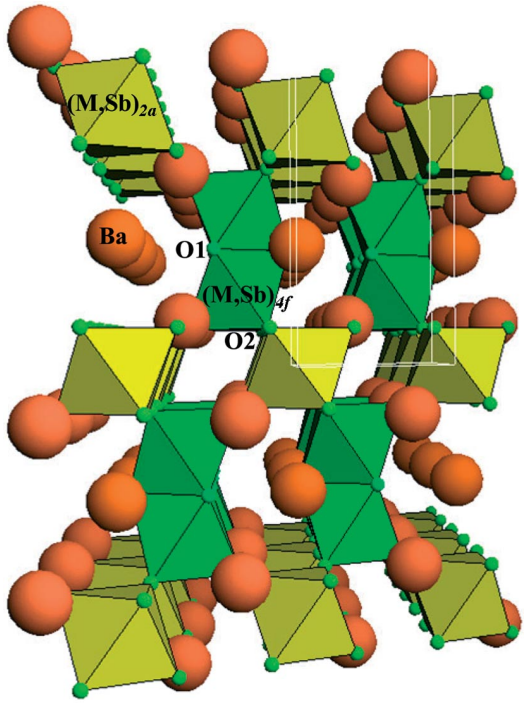

Figure 3. View of the crystal structure of hexagonal Ba_2MSbO_6 (M = Fe, Co), defined in the space group $P6_3/mmc$; c axis is vertical. $(M,Sb)_{4f}O_6$ octahedra (green) form dimer units sharing a common face through O1 oxygen atoms; these units are connected by $(M,Sb)_{2f}O_6$ octahedra (yellow) sharing corners through O2 oxygen atoms along the c axis. The Ba atoms are in 12-fold oxygen-coordinated cavities within the network of octahedra.

The thermal evolution of the crystal structure and the eventual establishment of a magnetic ordered phase was studied from the sequential D1B data in the temperature range T = 2–180 K for M = Fe and T = 2–95 K for M = Co. Figure 4 displays the NPD patterns sequentially obtained at these temperature regions. The low-temperature NPD diagrams do not show any magnetic contribution on the low-angle reflections, which could be ascribed to the establishment of a long-range magnetic ordering between the Fe or Co spins. Figure 5 presents the thermal variation in the unit-cell parameters for both compounds, which includes the D2B data at room temperature and D1A data at 97 and 191 K for M = Fe. There is an initial decrease in both the a and c parameters down to about 100 K, and then they exhibit an almost constant value down to 5 K. Although the absence of a magnetic contribution on the low-temperature patterns indicates that the long-range magnetic ordering, if any, is very weak, the thermal variation in the unit-cell parameters suggests some type of magneto-elastic coupling, which has already been described for several antiferromagnetic double perovskites.[13]

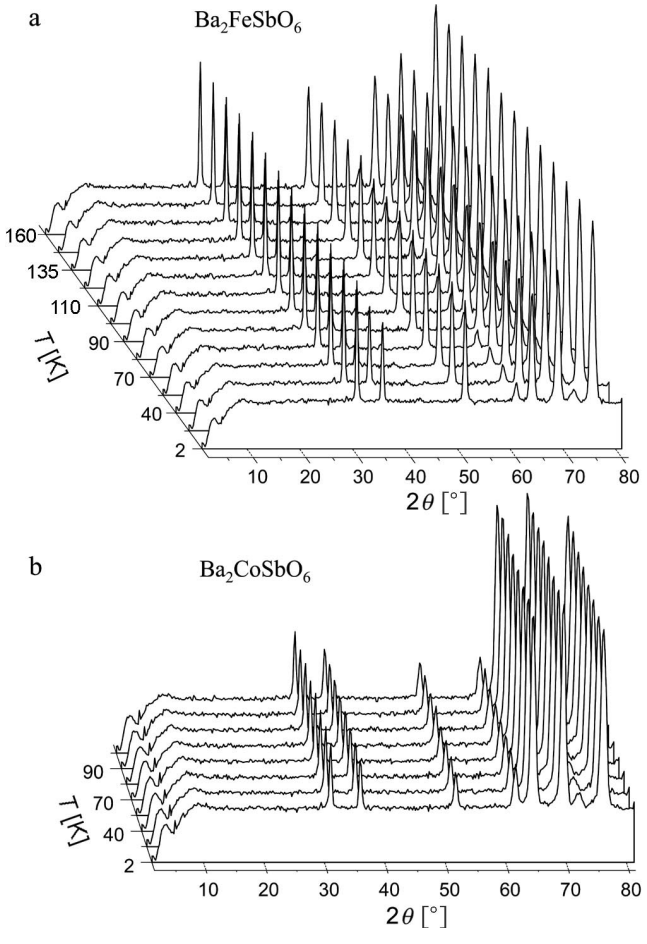

Figure 4. Thermal evolution of the NPD patterns collected with λ = 2.51 Å for (a) Ba_2FeSbO_6 and (b) Ba_2CoSbO_6.

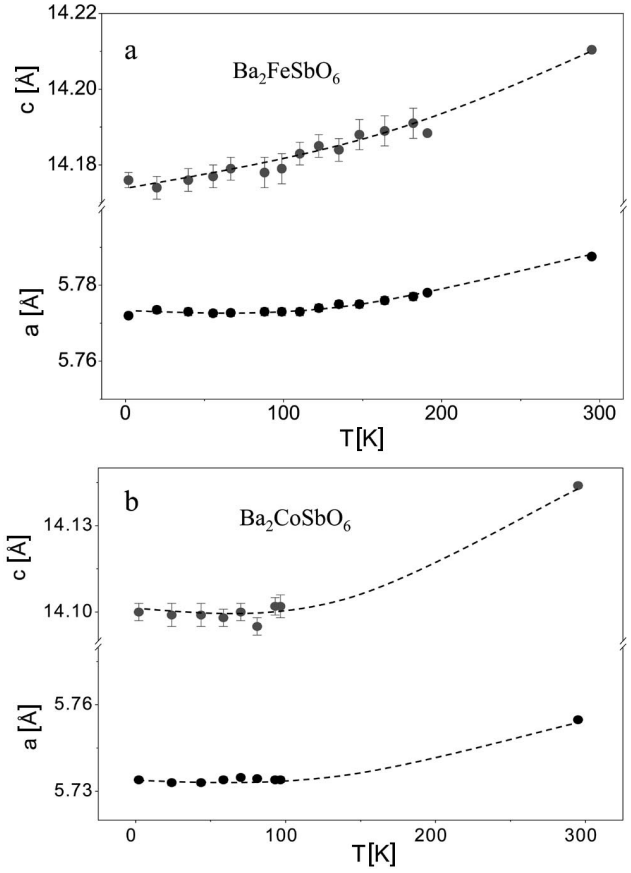

Figure 5. Thermal variation of the unit-cell parameters for (a) Ba_2FeSbO_6 and (b) Ba_2CoSbO_6.

Magnetic Data

The magnetization versus temperature curves are displayed in Figure 6a and Figure 7a for Ba_2FeSbO_6 and Ba_2CoSbO_6, respectively. They both show a rather similar pattern of behaviour; the FC susceptibility smoothly increases with cooling without showing any anomaly, which suggests the absence of a long-range magnetic ordering effect. For M = Fe, the ZFC and FC curves are not perfectly superimposed below 300 K and shows an additional divergence at 8 K (see inset in Figure 6). For M = Co, the ZFC and FC curves diverge below 14 K, which is characteristic, as in the case of Fe, of magnetic irreversibility. The reciprocal susceptibility data for M = Fe (right axis of Figure 6a) can be fitted to a Curie–Weiss law in the range 150–400 K, which gives a paramagnetic temperature Θ_{Weiss} = –116.6 K. This result suggests the presence of antiferromagnetic interactions. The value of the effective paramagnetic moment, μ_{eff} = 5.39 μ_B/f.u., is slightly lower than that expected for the electronic configuration $Fe^{3+}(3d^5)$–$Sb^{5+}[4d^{10}]$ (5.92 μ_B); the magnetism only arises from high-spin Fe^{3+} (S = 5/2). For M = Co, the reciprocal susceptibility shows a significant curvature (right axis of Figure 7a). A tentative Curie–Weiss fit in the 300–400 K temperature region gives Θ_{Weiss} = –248 K and an effective paramagnetic moment μ_{eff} =

4.4 μ_B/f.u., which is below that expected for the hypothetical electronic configuration $Co^{3+}(3d^7)$–$Sb^{5+}[4d^{10}]$ (4.90 μ_B) for high-spin Co^{3+} ($S = 2$), as will be discussed later on.

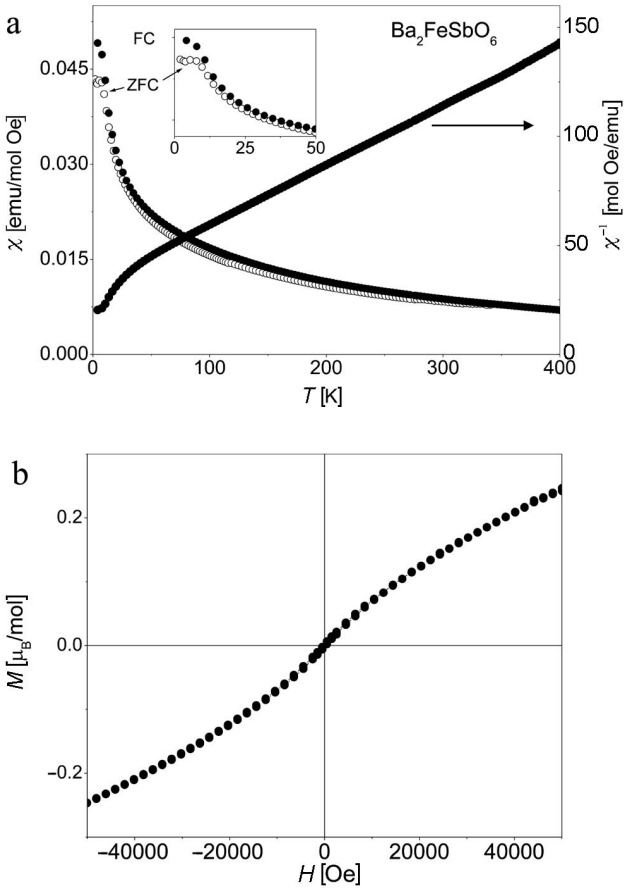

Figure 6. (a) Magnetic susceptibility (left axis) and reciprocal susceptibility (right axis) versus temperature curve for Ba_2FeSbO_6. The inset is a close-up of the low-temperature region. (b) Magnetization isotherm at 5 K.

The magnetization versus magnetic field curves at 5 K are plotted in Figure 6b and Figure 7b for Ba_2FeSbO_6 and Ba_2CoSbO_6, respectively. Both plots show a slight curvature of the magnetization, which is characterized by low saturation values. For H = 50 kOe, the maximum magnetization values are 0.25 μ_B/f.u. and 0.28 μ_B/f.u. for the Fe and Co compounds, respectively, although full saturation is not reached.

Mössbauer Data

The ^{57}Fe Mössbauer spectra of Ba_2FeSbO_6 recorded at 295 K and 77 K are shown in Figure 8a and b, respectively. The parameters of the fitted spectra corresponding to the isomer shift (IS), quadrupole splitting (QS), full width at half maximum (FWHM) and relative spectral area of the absorber resonance lines are shown in Table 3. In agreement with the NPD data and magnetic measurements, the spectra do not reflect any magnetic ordering in the sample studied down to 77 K. Both spectra were fitted by superposition of

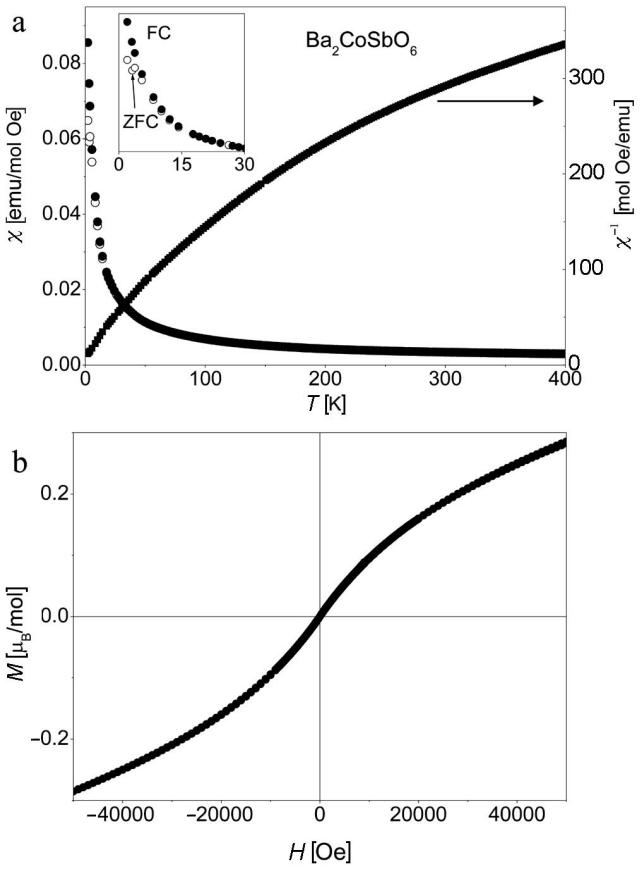

Figure 7. (a) Magnetic susceptibility (left axis) and reciprocal susceptibility (right axis) versus temperature curve for Ba_2CoSbO_6. The inset is a close-up of the low-temperature region. (b) Magnetization isotherm at 5 K.

two components: a broaden singlet (*2a*) and a continuous distribution of quadrupole doublets (*4f*). For this latter spectral component the values of the isomer shift, quadrupole splitting, and full width at half maximum shown in Table 3 should be considered as average values of individual quadrupole doublets. Within experimental error, any change in the quadrupole splitting at 77 K that is characteristic of Fe^{3+} valence in the investigated material was not observed. By lowering the temperature, the relative spectral area of the absorber resonance lines do not change, which indicates that the factors of recoilless fraction for the two sites of Fe^{3+} are equal as well. One should mention the slightly lower occupancy of iron in the deformed *4f* sites detected by the Mössbauer spectroscopic method (ideally 66%), which is in overall agreement with the NPD findings for an ordering degree of 6% of the Fe perovskite.

Table 3. Mössbauer parameters for Ba_2FeSbO_6 at 295 and 77 K.

T [K]	Component	IS [mm/s]	QS [mm/s]	FWHM [mm/s]	Rel. spectral area [%]
295	*2a* site	0.34 ± 0.01	0	0.25 ± 0.02	39.3 ± 1.5
	4f site	0.34 ± 0.01	0.74 ± 0.02	0.23 ± 0.02	60.7 ± 1.5
77	*2a* site	0.45 ± 0.01	0	0.25 ± 0.01	39.8 ± 1.2
	4f site	0.45 ± 0.01	0.73 ± 0.01	0.23 ± 0.01	60.2 ± 1.2

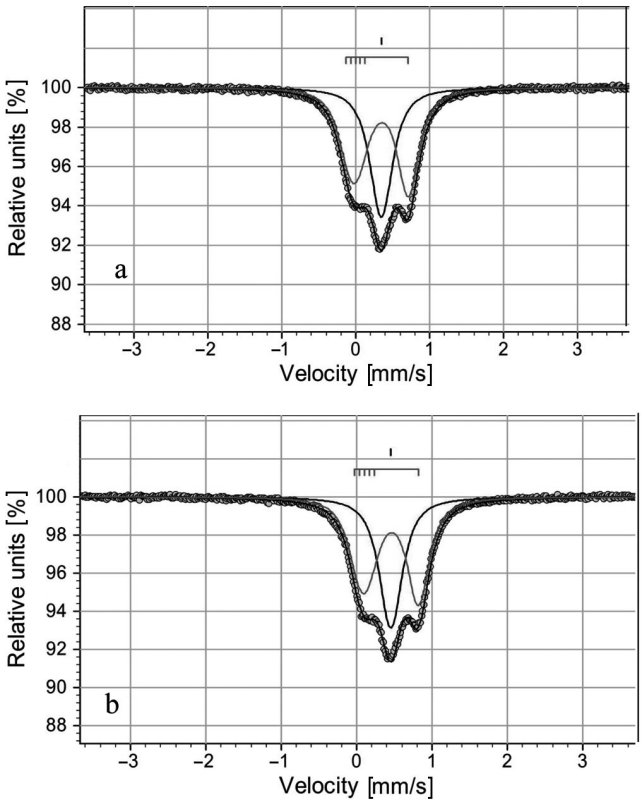

Figure 8. Mössbauer spectra for Ba_2FeSbO_6 collected at (a) 295 K and (b) 77 K.

Discussion

As demonstrated from the high resolution NPD study, both Ba_2MSbO_6 perovskites display a severe M/Sb long-distance disorder with degrees of ordering of 6% for M = Fe and 28% for M = Co. This low-grade long-range cationic ordering reflects a trend observed for double perovskites in which charge differences higher than 2 are generally needed to obtain a high degree of cationic order. If we normalize the crystallographic formula into the standard $A_2B'B''O_6$ nomenclature, we obtain $Ba_2FeSbO_{5.92(4)}$ and $Ba_2CoSbO_{5.80(4)}$. We can consider that the Fe perovskite has stoichiometric amounts of oxygen (within 2 standard deviations). This fact is further supported by Mössbauer spectroscopy, where only Fe^{3+} cations were detected, whereas the Co compound shows a non-negligible oxygen deficiency, which indicates a mixed-valence state for cobalt: 40% Co^{2+}/60% Co^{3+}. The fact that the Co perovskite is substantially more ordered is certainly related to the presence of divalent Co cations in the structure. The current preparation conditions, which involve thermal treatment in air, do not provide the required oxidizing power to complete the oxygen sublattice and promote the stabilization of 100% Co^{3+}. This fact is in agreement with the observation by Primo-Martin et al.[14] who prepared the Sr analogue Sr_2CoSbO_6 under 3 kbar O_2 pressure. However, they stabilized $Sr_2CoSbO_{5.63}$ by solid-state reactions in air, and the compound also contained a substantial amount of Co^{2+} cations.

Unlike the so-called 3C-type perovskite structures[15] observed for tolerance factors $t \leq 1$ and characterized by a three-dimensional network of corner-sharing BO_6 octahedra, the present Ba_2MSbO_6 phases belonging to the 6-layered, 6H-type perovskite structures exhibit a distinct stacking of the M/Sb octahedra, as illustrated in Figure 3. In the structure, couples of $(M,Sb)_{4f}O_6$ octahedra containing a random distribution of M and Sb cations are linked by a common face through the O1 oxygen atoms to give dimer units, which exhibit $(M,Sb)_{4f}$–O1–$(M,Sb)_{4f}$ angles of 85° (M = *F*e) or 82° (M = Co) at room temperature. The direct distances $(M,Sb)_{4f}$–$(M,Sb)_{4f}$ are rather short, with a value of 2.827(3) Å (M = Fe) or even shorter for M = Co [2.652(9) Å]. The dimers are connected to the $(M,Sb)_{2a}O_6$ octahedra (also containing a random distribution of M and Sb atoms) through the corners by O2 oxygen atoms. Whereas the $(M,Sb)_{2a}O_6$ octahedra are perfectly regular with respect to the (M,Sb)–O distances, the octahedral units within the dimers are deformed along the *c* axis and show significantly longer $(Fe,Sb)_{4f}$–O1 bonds along this direction (2.091 Å) than the $(Fe,Sb)_{4f}$–O2 bonds [1.950(3) Å] at room temperature, probably as a result of the repulsive effect of the cations throughout the octahedral faces. The same is observed for the Co compound, with longer $(Co,Sb)_{4f}$–O1 bonds along the *c* axis [2.013(5) Å] than the $(Co,Sb)_{4f}$–O2 bonds [1.984(6) Å], although the difference is much smaller in this case. The fact that the $(Co,Sb)_{4f}O_6$ octahedra are significantly less deformed is certainly related to the lower Sb^{5+} occupancy at these positions for the Co compound; the repulsion between the highly charged Sb^{5+} cations is the main driving force for the octahedral deformation. This is a direct consequence of the higher degree of M/Sb ordering observed for the Co compound, in which Sb is concentrated at the layers of $(M,Sb)_{2a}O_6$ octahedra away from the dimer units. This is related to the substantially smaller metal–metal distance within the dimers, which experience a reduced repulsion across the common faces of the $(Co,Sb)_{4f}O_6$ octahedra along the *c* axis. Moreover, the considerably smaller *c* unit-cell parameter of Ba_2CoSbO_6 (14.144 Å at room temperature) relative to Ba_2FeSbO_6 (14.210 Å at room temperature) is also associated with the lower antisite disorder observed for the Co perovskite. It is also interesting to note that the oxygen deficiency of this perovskite is mainly associated with the O1 oxygen atoms (Table 1) linking together the *4f* octahedra in which there exists a larger ratio of Co cations, some of them (40%) exhibiting a lower oxidation state of +2. The absence of these oxygen atoms is also associated with the partial collapse of the crystal structure along the *c* axis, relative to the Fe compound.

The Mössbauer spectra of Ba_2FeSbO_6 (Figure 8) were fitted using a superposition of two components: a broad singlet (*2a*) and a continuous distribution of quadrupole doublets (*4f*). As just mentioned, the *2a* octahedron is regular and the surrounding oxygen ions should not create an electric field gradient at the centred Fe ion. However, the random distribution of the so-called next-nearest neighbours (Fe or Sb) leads to a significant broadening of the singlet. The second component has to be attributed to *4f*

deformed octahedra, where the impact of the randomly distributed next-nearest neighbours leads to a distribution of quadrupole doublets. Previously, Battle et al.[12] observed, from a Mössbauer study, a Fe distribution where most of the Sb was placed at the dimer positions, which could be surprising since this arrangement maximizes the repulsion between the Sb^{5+} cations. Our NPD study demonstrates that Fe and Sb are almost randomly distributed over both sites, which is corroborated by the present Mössbauer investigation in which a 61(2)% Fe occupancy at *4f* sites and 39(2)% occupancy at *2a* positions is observed, according to the multiplicity and the slightly superior occupancy of Fe at the *2a* sites.

In contrast with the Sr_2FeMoO_6 double perovskite, a paradigmatic example of half-metallic and ferromagnetic perovskite that must be prepared under reducing conditions in order to provide a mixed valence Fe^{3+}/Fe^{2+}–Mo^{5+}/Mo^{6+} state,[1] the present Ba_2FeSbO_6 perovskite has been synthesized in air in such a way that, from the chemical point of view, we should assign a nominal pentavalent oxidation state to the Sb cations as the Fe cations are nominally trivalent, as demonstrated in the Mössbauer study. From this point of view, the electronic configuration for this sample would be $Fe^{3+}(3d^5)$–$Sb^{5+}(4d^{10})$. A confirmation of these valence states is obtained from the average size of the octahedra. Ba_2FeSbO_6 exhibits a similar size of 2.02 Å for both *2a* and *4f* octahedral units (Table 2), for which the expected distances based upon the average sums of ionic radii[16] for high-spin Fe^{3+} (0.641 Å) and Sb^{5+} (0.60 Å) with O^{2-} (1.40 Å) gives exactly the observed value.

The absence of an additional scattering contribution evident in the low-temperature NPD diagrams, which indicates the lack of long-distance ordering of the Fe^{3+} spins, should be as a result of the almost random distribution of Fe over the two octahedral sites. It is pertinent to mention the examples of two closely related double perovskites, Sr_2FeTaO_6 and Sr_2FeSbO_6.[17] The former compound, characterized by a totally random distribution of Fe/Ta cations over the B positions of the 3C-type perovskite (with a *Pbnm* space group), shows no evidence of long-range magnetic ordering and exhibits a spin-glass behaviour below 23 K. For Ba_2FeSbO_6, we observe a similar divergence in the ZFC and FC curves, which also suggests the presence of a spin glass. The second example, Sr_2FeSbO_6,[17] displays a considerably lower antisite disordering (roughly 80% of Fe at Sb positions and vice versa), and the NPD data show the coexistence of a magnetically ordered spin system and a spin-glass system. In our case, the observation of a slight curvature in the magnetization isotherms is symptomatic of a certain level of short-range ordering, perhaps by polarization of the spins under a relatively strong (up to 5 T) external magnetic field, which is undetectable by neutron diffraction.

For $Ba_2CoSbO_{5.80(4)}$, the interpretation of the magnetic properties is more complex, given the presence of a mixed valence state for Co: 40% Co^{2+}/60% Co^{3+}. The existence of several spin states for Co^{3+} ($3d^6$) has been known for years. In the paradigmatic example of $RCoO_3$ perovskites, the occurrence of low-spin Co^{3+} (LS, $S = 0$) in the low-temperature region is followed by a transition to intermediate spin ($S = 1$) and finally to high spin (HS, $S = 2$), at increasing temperatures as the rare earth metal size becomes smaller.[18] The spin state depends on the strength of the crystal field experienced by Co^{3+} in an octahedral coordination: the HS state ($t_{2g}^4e_g^2$) is achieved in weak octahedral ligand fields, whereas the LS state (t_{2g}^6) occurs in strong fields, as it is often observed, for instance, in complex fluorides. The intermediate spin state ($t_{2g}^5e_g^1$) occurs as the ground state in lower symmetries such as axially distorted octahedra.[19] For $Ba_2CoSbO_{5.80(4)}$, it is highly improbable that a LS state for Co^{3+} (60% of Co atoms) occurs since the presence of Sb^{5+} ions over the same crystallographic sites provides a strong polarization to the oxygen atoms in Sb–O–Co configurations such that the crystal field provided by the O ligands bonded to the Co cations is considerably reduced, which therefore enhances the thermal promotion of higher spin states. Similar conclusions were drawn for Sr_2CoSbO_6 (containing 100% Co^{3+}),[14] for which it was stated that no pure LS Co^{3+} is attained even at lower temperatures, contrary to that observed for $LaCoO_3$ and $YCoO_3$, among others. In the present case, if we consider the pertinent proportion of high-spin Co^{2+} with spin-only contribution ($S = 3/2$) with an admixture of high-spin Co^{3+} ($S = 2$), we should expect an effective moment of 4.51 μ_B/f.u., which is in reasonably good agreement with our Curie–Weiss determination of the effective paramagnetic moment, $\mu_{eff} = 4.4\ \mu_B$/f.u. Moreover, the curvature observed in the reciprocal susceptibility curve for $Ba_2CoSbO_{5.80(4)}$ could be due to the progressive population of the higher spin states promoted by thermal activation as the temperature increases. It is interesting to compare the calculated octahedral average sizes of the octahedral units at the *2a* and *4f* sites with the sum of the ionic radii[16] for the proposed admixture of HS Co^{2+} (0.745 Å), HS Co^{3+} (0.578 Å as average of tabulated HS and LS Co^{3+}) and Sb^{5+} (0.60 Å); a value of 2.03 Å, which compares with the observed value of 2.00 Å for both octahedral positions, is obtained.

The absence of long-range magnetic ordering in $Ba_2CoSbO_{5.80(4)}$ can also be explained, as in the case of the Fe perovskite, as a result of the formation of a spin-glass state, which is supported by the irreversible behaviour of the ZFC versus FC measurements. As indicated before, typical spin-glass transitions result from the existence of different exchange interactions that are competing and hence giving rise to a certain degree of magnetic frustration.[20] This is usually found in disordered structures and, in particular, in perovskites where some degree of disorder is achieved for the magnetic ion. An illustrative example is the Ba_2CoNbO_6 perovskite,[21] which has been described as a cubic aristotype structure ($Pm\bar{3}m$) with a completely disordered arrangement of the B cations and shows a spin-glass transition that originates from the magnetic frustration due to the coexistence of intermediate spin and HS Co^{3+} states together with Nb over the B positions. Further, the more similar example of Sr_2CoSbO_6,[14] with rhombohedral symmetry ($R\bar{3}m$), was described to experience a spin-glass tran-

sition at 47 K, in spite of showing a partial order (77%) of the B cations. The defective perovskite $Sr_2CoSbO_{5.63}$ exhibits an even lower spin-glass transition temperature at 17 K. In the present case, the observation of the slight curvature in the magnetization isotherms at 5 K indicates some short-range interactions, which lead to the appearance of a small neat magnetization, perhaps arising from a subtle canting of the magnetic moments upon application of an external magnetic field. However, these interactions are undetectable by NPD techniques.

Conclusions

The crystal structures of $Ba_2MSbO_{6-\delta}$ (M = Fe, Co) have been refined from NPD data in the $P6_3/mmc$ space group and contain two kinds of octahedral positions; both positions contain a random distribution of M and Sb cations, and the structures exhibit a poor long-range cationic ordering. The M = Fe perovskite is 6% ordered, whereas the Co compound is considerably more ordered (28%) because of the presence of oxygen vacancies and hence the Co^{2+} state (40%). Within the layered 6H crystal structure, the $(M,Sb)_{4f}O_6$ octahedral units, which form dimer units sharing common faces, are axially distorted, as demonstrated by NPD data and confirmed by Mössbauer spectroscopy for Ba_2FeSbO_6; this distortion is driven by the direct repulsion between the (M,Sb) cations within the dimer, which is partially screened by the triangular faces of O1 oxygen atoms. This repulsion is lower for the Co compound, which contains a smaller ratio of Sb^{5+} in the dimers as a consequence of the superior cationic ordering for this oxide. The second type of octahedra, $(M,Sb)_{2a}O_6$, are linked to the dimers by common corners (O2 oxygen atoms) and are perfectly regular, as also confirmed by Mössbauer spectroscopy for Ba_2FeSbO_6. The magnetic properties as well as the low-temperature NPD patterns suggest the absence of long-range magnetic ordering with the formation of spin-glass states for both compounds. Nevertheless, the non-zero magnetization observed at 5 K indicates some short-range interactions, which lead to the appearance of a small neat magnetization, perhaps arising from a subtle canting of the magnetic moments upon application of an external magnetic field.

Experimental Section

Ba_2MSbO_6 (M = Fe, Co) were prepared as brown (M = *F*e) or black (M = Co) polycrystalline powders by solid-state reactions. Stoichiometric amounts of analytical grade $BaCO_3$, $Fe(NO_3)_3 \cdot 6H_2O$ and Sb_2O_3 were mixed, ground, placed in an alumina crucible and slowly heated (180 °C h^{-1}) to 1100 °C to minimize Sb_2O_3 evaporation, and then held at this temperature for 12 h. This procedure yielded a pure perovskite phase for M = Fe; for M = Co, additional treatment at 1150 °C for 8 h was required with intermediate regrinding. The initial structural identification and characterization of the samples was carried out by XRD (Cu-K_α, λ = 1.5418 Å).

The magnetic measurements were performed with a commercial SQUID magnetometer. The susceptibility was measured under zero-field cooling (ZFC) and field cooling (FC) conditions under a 1 kOe magnetic field for temperatures ranging from T = 2–350 K. Isothermal magnetization curves were obtained at T = 5 K under an applied magnetic field that varied from –50 to 50 kOe.

NPD data were acquired at the Institut Laue-Langevin in Grenoble (France). For the study of the crystallographic structure, NPD patterns for both samples were collected at room temperature (295 K) with the D2B diffractometer with a wavelength of 1.594 Å; additionally two more patterns were acquired for M = Fe at T = 97 K and 191 K with the D1A medium-resolution diffractometer with λ = 1.910 Å. For the study of the eventual magnetic structure and the analysis of its thermal evolution, a set of NPD patterns were collected with the D1B diffractometer with λ = 2.505 Å in the temperature range T = 2–180 K for M = Fe and T = 2–95 K for M = Co. A standard "orange" cryostat was used for the sequential collections. The experimental NPD patterns were analyzed by the Rietveld method[22] with the FULLPROF program.[23] For the refinements, the shape of the peaks was simulated by a pseudo-Voigt function, and the background was fitted by a fifth-degree Chebyshev polynomial. The coherent scattering lengths for Ba, Fe, Co, Sb and O were 5.07, 9.45, 2.49, 5.57 and 5.803 fm, respectively. In the final runs, the following parameters were refined: scale factor, background coefficients, zero-point error, unit-cell parameters, pseudo-Voigt corrected for asymmetry parameters, positional coordinates, isotropic thermal factors, relative M/Sb occupancy factor and oxygen occupancy factors (D2B data only).

The sample for the Mössbauer spectroscopic study was prepared by mixing powdered Ba_2FeSbO_6 with polyvinyl alcohol powder, which was then pressed into a disc with a diameter of 12 mm. The optimum thickness of the disc was chosen to have 5.3 mg/cm^2 Fe. The Mössbauer spectroscopic analysis was performed at 300 and 77 K in transmission mode with a conventional constant acceleration spectrometer. A ^{57}Co source in a Rh matrix with a activity of 100 mCi and a diameter of the activity spot of 5 mm was used. The spectra were fitted by using an integral Lorentzian line-shape approximation. This approach permits the separation of the absorber line and avoids the thickness effect.[24,25] The isomer shifts of the spectra were referred to the centroid of an α-Fe foil (25 μm) reference spectrum at room temperature. The geometric effect due to the source motion was taken into account as well.

Acknowledgments

We thank the CICyT for financial support through the project MAT2007-60536 and ILL for the use of their facilities. We are grateful for the financial support provided by a CSIC-BAS collaboration project.

[1] K.-I. Kobayashi, T. Kimura, H. Sawada, K. Terakura, Y. Tokura, *Nature* **1998**, *395*, 677.
[2] K.-I. Kobayashi, T. Kimura, Y. Tomioka, H. Sawada, K. Terakura, Y. Tokura, *Phys. Rev. B* **1999**, *59*, 11159.
[3] T. H. Kim, M. Uehara, S. W. Cheong, S. Lee, *Appl. Phys. Lett.* **1999**, *74*, 1737.
[4] A. P. Ramirez, *J. Phys. Condens. Matter* **1997**, *9*, 8171.
[5] C. N. R. Rao, B. Raveau (Eds.), *Colossal Magnetoresistance, Charge Ordering And Related Properties Of Manganese Oxides*, World Scientific, Singapore, **1998**.
[6] M. Retuerto, J. A. Alonso, M. García-Hernández, M. J. Martínez-Lope, *Solid State Commun.* **2006**, *139*, 19.

[7] M. Retuerto, M. García-Hernández, M. J. Martínez-Lope, M. T. Fernández-Díaz, J. P. Attfield, J. A. Alonso, *J. Mater. Chem.* **2007**, *17*, 1.
[8] R. D. Burbank, H. T. Evans Jr, *Acta Crystallogr.* **1948**, *1*, 330.
[9] F. Sher, J. P. Attfield, *Solid St. Sci.* **2006**, *8*, 277.
[10] G. Blasse, *J. Inorg. Nucleic Chem.* **1965**, *27*, 993.
[11] G. Blasse, *Philips Res. Repts.* **1965**, *20*, 327.
[12] P. D. Battle, T. C. Gibb, A. J. Herod, S.-H. Kim, P. H. Munns, *J. Mater. Chem.* **1995**, *5*, 865.
[13] M. J. Martínez-Lope, J. A. Alonso, M. T. Casais, M. T. Fernández-Díaz, *Eur. J. Inorg. Chem.* **2002**, 2463.
[14] V. Primo-Martín, M. Jansen, *J. Solid St. Chem.* **2001**, *157*, 76.
[15] A. F. Wells (Ed.) in *Structural Inorganic Chemistry*, Clarendon Press, Oxford, 5th ed., **1984**, pp. 582–583.
[16] R. D. Shannon, *Acta Crystallogr., Sect. A* **1976**, *32*, 751.
[17] E. J. Cussen, J. F. Vente, P. D. Battle, T. C. Gibbs, *J. Mater. Chem.* **1997**, *7*, 459.
[18] K. Asai, A. Yoneda, O. Yokokura, J. M. Tranquada, G. Shirane, K. Hohn, *J. Phys. Soc. Jpn.* **1998**, *67*, 290.
[19] B. Buffat, G. Demazeau, M. Pouchard, P. Hagenmuller, *Proc. Indian Sacad. Sci.* **1984**, *93*, 313.
[20] K. Moorjani, J. M. D. Coey, *Magnetic Glasses*, Elsevier, Amsterdam, **1984**, p. 36.
[21] K. Yoshii, *J. Solid State Chem.* **2000**, *151*, 294.
[22] H. M. Rietveld, *J. Appl. Crystallogr.* **1969**, *2*, 65.
[23] J. Rodríguez-Carvajal, *Phys. B* **1993**, *192*, 55.
[24] G. K. Shenoy, J. M. Friedt, H. Maleta, S. L. Ruby in *Mössbauer Effect Methodology*, **1974**, vol 9, p. 277.
[25] T. E. Cranshaw, *J. Phys. E* **1974**, *7*, 122.

Received: January 16, 2008
Published Online: April 4, 2008

